Polymer Journal (2022) 54:293–303
https://doi.org/10.1038/s41428-021-00563-2

ORIGINAL ARTICLE

# Thermo-driven self-healable organic/inorganic nanohybrid polyurethane film with excellent mechanical properties

Haoliang Wang[1,2] · Hui Wang[1] · Junhuai Xu[1] · Xiaosheng Du[1] · Shiwen Yang[3] · Haibo Wang[1,2]

Received: 17 July 2021 / Revised: 16 August 2021 / Accepted: 26 August 2021 / Published online: 30 November 2021


## Abstract

Waterborne polyurethane (WPU) is widely applied in many fields; however, it is limited by its drawback of low mechanical strength and short lifespan. Polymer nanocomposites have been developed for many years to enhance the mechanical behavior of materials. Nevertheless, obtaining nanofillers with even dispersion to obtain improved mechanical performance is difficult. To solve the above problems, silica nanoparticles modified by furfuryl (furan@$SiO_2$) were synthesized according to the sol–gel process. By introducing furan@$SiO_2$ into a maleimide-terminated waterborne polyurethane matrix, a self-healing system was constructed through a DA/retro-DA process among furan groups and maleimide-terminated waterborne polyurethane, and a series of WPU films with different furan@$SiO_2$ (WMPUS-x) contents were prepared. The structure of furan@$SiO_2$ was clearly corroborated by TEM, SEM, FTIR, etc. Moreover, confirmed by tensile tests, the mechanical properties of all WPU samples were significantly improved due to the addition of rigid furan@$SiO_2$, and their first self-healing efficiencies were all higher than 88%.

## Introduction

As a consequence of low volatile organic compound (VOC) release, waterborne polyurethane (WPU) is in line with the trend of advocating for environmental protection and gradually replacing traditional solvent-based polyurethane. WPU, which possesses excellent low-temperature resistance, convenient transportation and nonflammability properties, has been widely applied in commercial fields such as organic coatings, fabric finishing agents, and adhesives [1, 2]. At present, a need is apparent for further WPU development, not least with regard to greater consideration of the main defects, such as low mechanical strength and poor water resistance [3, 4]. Many efforts have been made to disperse nanoparticles into polymer matrices. Rigid nanoparticles have excellent corrosion resistance, high temperature resistance and oxidation resistance [5, 6]. Therefore, it is not uncommon to introduce nanofillers into polymer systems, giving rise to the mechanical properties and thermal stability of polymer-based materials [7–9]. However, the fact that the addition of nanoparticles in some cases, on the contrary, causes adverse effects on the mechanical performance of polymers is due first to interfacial compatibility between nanofillers and the polymer matrix and second to the inhomogeneous dispersion of nanoparticles.

To intensify the compatibility between the nanofillers and WPUs, an effective way is to modify the surface of inorganic nanofillers with organic groups such as mercapto and furan groups, which can eliminate the interfacial energy difference and maintain good affinity with the matrix [10, 11]. As a result, the mechanical properties of the polymer composites can be significantly enhanced. Although inspiring progress has been made, there are still

These authors contributed equally: Haoliang Wang, Hui Wang.

**Supplementary information** The online version contains supplementary material available at https://doi.org/10.1038/s41428-021-00563-2.

✉ Shiwen Yang
swyang@wtu.edu.cn

✉ Haibo Wang
whb6985@scu.edu.cn

[1] College of Biomass Science and Engineering, Sichuan University, Chengdu 610065, PR China

[2] The Key Laboratory of Leather Chemistry and Engineering (Sichuan University), Ministry of Education, Chengdu 610065, PR China

[3] College of Materials Science and Engineering, State Key Laboratory of New Textile Materials & Advanced Processing Technology, Wuhan Textile University, Wuhan 430200, China

some aspects waiting for improvement. Due to the high specific surface energy and strong hydrogen bonding of nanoparticles, it is difficult to obtain monodisperse nanoparticles only by surface modification. The agglomeration of nanofillers is the key factor restricting the improvement and progress of polymer nanocomposites. Hence, it is necessary to find a simple approach to increase the grafting rates of organic groups and thus effectively prevent the agglomeration phenomenon.

To the best of our knowledge, the sol–gel method provides a considerable method for the homogeneous mixing of organic and inorganic phases at the molecular level [12, 13], and the poor dispersion of nanofillers in polymer matrices can also be ameliorated. It is well known that different catalytic conditions are responsible for the diverse products of siloxane formed via a sol–gel reaction. Unlike the chain-like structure formed under acidic catalysis, siloxane tends to condense, forming globular structured rigid particles under alkaline catalysis, which surmounts the uniform dispersion and thus ensures interfacial stress transfer from the matrix to the filler [14, 15]. Therefore, organic-modified silica nanoparticles, as an ideal material for reinforcing the properties of polymers, can be obtained through an alkaline catalytic sol–gel process.

However, only enhancing the mechanical behavior of WPU by no means satisfies the demand of modern industrial fields. Cracks often develop inside or on the surface of WPU during use, which can cause catastrophic security problems or shorten the lifespan of WPU. Consequently, it is necessary to endow WPU products with self-healing ability by molecular design [16, 17]. The introduction of reversible or dynamic covalent bond structures into polymers is a familiar scheme to construct intrinsically stimuli-responsive self-healing systems [18, 19]. Currently, numerous self-healing materials have been successfully prepared via reversible chemical changes, such as DA reactions [20], anthracene dimerization [21], coumarin dimerization [22], and disulfide exchange [23]. Among these reversible chemical reactions, DA/retro-DA reversible reactions are the best known. The [4 + 2] cycloaddition DA reaction involves a diene (usually a furan) and a dienophile (usually a maleimide) at moderate temperature. Stimulated by elevated temperature, the corresponding diene and dienophile are regenerated via a retro-DA reaction [24]. Since the DA reaction is advantageous in that it is simple, readily reversible, and effective and produces few side reactions [25], it provides a feasible method to prepare polymer materials with excellent self-repairing ability through a retro-DA/DA process [26, 27].

In this work, homogeneously dispersed furfuryl-modified silica nanoparticles (furan@$SiO_2$) were synthesized according to the alkaline catalytic sol–gel process. Various characterizations confirmed that the furan@$SiO_2$ particles were inorganic–organic hybrid particles that not only possessed the rigidity of inorganic particles but also exhibited single dispersion properties. By adding furan@$SiO_2$ to a maleimide-terminated WPU emulsion, a reversible cross-linking network was formed between furan@$SiO_2$ and WPU via thermally triggered DA/retro-DA reactions. The furan@$SiO_2$ particles, which possessed high furan group grafting rates and acted as dynamic cross-linking points, significantly enhanced the strength of WPU by sufficient cross-linking. Due to the construction of an intrinsically stimulus-responsive self-healing system via the DA/retro-DA reaction, inorganic–organic hybrid nanoparticles/maleimide-terminated waterborne polyurethane (WMPUS-x) showed a high thermo-driven self-healing efficiency, even during multiple healing processes. Moreover, the effects of different hybrid nanoparticle contents on the mechanical properties, thermal stability and self-healing behavior of WMPUS-x were systematically investigated. It is not surprising that WMPUS-x will show excellent comprehensive performance.

## Experimental

### Materials

Materials used in this research included 3-methacryloxypropyltrimethoxysilane (γ-MPS, ≥98.0%, Best-reagent, China), furfuryl mercaptan (Fu-SH, 98.0%, Best-reagent, China), N,N-diethylethanamine (TEA, ≥99.0%, Kelong Reagent Co., Ltd, China), tetraethyl orthosilicate (TEOS, 99.0%, Kelong Reagent Co., Ltd, China), ammonium hydroxide ($NH_4OH$, 0.88 g $mL^{-1}$, Kelong Reagent Co., Ltd, China), poly(propylene glycol) (PPG2000, Mn = 2000 g $mol^{-1}$, Wanhua Chemical Group Co., Ltd, China), 5-isocyanato-1-(isocyanatomethyl)-1,3,3-trimethylcyclohexane (IPDI, ≥99.5%, Wanhua Chemical Group Co., Ltd, China), dibutyltin dilaurate (DBTDL, Hersbit Chemical, China), butane-1,4-diol (BDO, ≥99.0%, Kelong Reagent Co., Ltd, China), 2,2-bis(hydroxymethyl)propionic acid (DMPA, Kelong Reagent Co., Ltd, China), maleic anhydride (MAH, 99.0%, Kelong Reagent Co., Ltd, China), furan (Best-reagent, China), ethanolamine (MEA, ≥99.0% Best-reagent, China), N-(2-hydroxyethyl) maleimide (HEMI, synthesized by our laboratory) (see ESI† for details), ethyl acetate (EAC), methylbenzene (≥99.0%), ethanol (≥99.0%), acetone (≥99.0%) and other solvents were received from Kelong Reagent Co., Ltd. (Chengdu, China). All reagents were completely dehydrated before use.

### Fabrication of inorganic–organic hybrid nanoparticles (furan@$SiO_2$)

The inorganic–organic hybrid nanoparticles were prepared by the sol–gel method as follows. First, γ-MPS, TEA, and

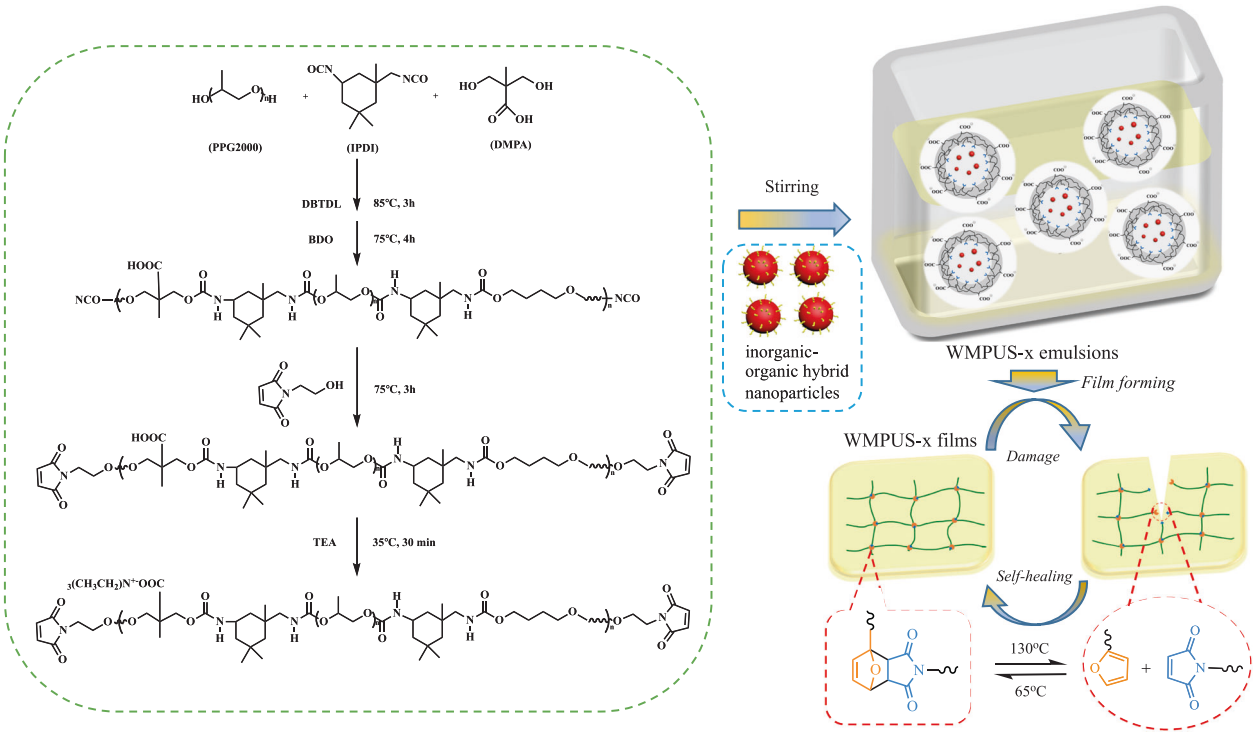


**Scheme. 1** Preparation route of WMPUS-x films

ethanol were mixed at room temperature at a molar ratio of 1:1.5:10 and stirred vigorously to obtain a homogeneous γ-MPS ethanol dispersion. Then, Fu-SH was added dropwise with a 1.03 molar excess of γ-MPS and stirred for 8 h at room temperature. Subsequently, a calculated amount of TEOS (γ-MPS:TEOS molar ratio of 3:1) was added to the above mixture, stirred well and hydrolyzed at 60 °C for 4 h. According to our many attempts, a higher molar ratio was conducive to ensuring the molar concentration of furan groups in furan@$SiO_2$, and furan@$SiO_2$ with high storage stability was also obtained. At the end of the reaction, the precipitate was aged at room temperature for 24 h. The precipitate was collected by centrifugation and washed several times with ethanol to remove unreacted Fu-SH. The final precipitate was dried in an oven at 40 °C for 24 h to obtain furan@$SiO_2$, which presented light yellow particles. The synthetic route is shown in Scheme S1.

## Preparation of the inorganic–organic hybrid nanoparticle/maleimide-terminated waterborne polyurethane (WMPUS-x) emulsion

Dehydrated PPG2000, IPDI and DMPA were added into a three-necked flask equipped with a condenser and agitator, and a certain amount of DBTDL catalyst was added. The mixture was heated to 85 °C, and the -NCO-blocked oligomer was obtained after 3 h. Subsequently, the temperature was lowered to 75 °C, and the chain extender BDO was added, together with an appropriate amount of acetone to reduce the reaction viscosity. The reaction continued for 4 h at 75 °C until the polyurethane prepolymer reached the theoretical NCO content. Next, a high-concentration acetone solution of HEMI was added to the prepolymer for blocking with a reaction time of 3 h. Once completed, the temperature was cooled to 35 °C, and TEA was added to neutralize for 30 min. The neutralized prepolymer was homogeneously mixed with a certain amount of prepared furan@$SiO_2$ and emulsified at high speed in deionized water to obtain a maleimide block waterborne polyurethane (WMPUS-x) emulsion with furan@$SiO_2$. The acetone solvent was removed under vacuum by using a rotary evaporator in a 45 °C water bath. The synthetic formulations are shown in Table S1. The preparation route of the WMPUS-x emulsion is illustrated in Scheme 1.

## Preparation of thermoreversible self-healing waterborne polyurethane (WMPUS-x) films

WMPUS-x films were obtained by pouring WMPUS-x emulsions on a Teflon mold and drying at room temperature for 48 h, followed by drying at 40 °C for 48 h and 60 °C for 24 h to obtain yellow films with a thickness of 0.5 ± 0.1 mm. According to the mass fraction of furan@$SiO_2$ in emulsions of 0 wt%, 2 wt%, 4 wt%, and 7 wt%, the prepared films were named WMPUS-0, WMPUS-1, WMPUS-2, and WMPUS-3, respectively.

## Characterization

Fourier transform infrared (FTIR) spectra were used to analyze the structure of samples and were recorded by a Nicolet 560 (USA) Fourier infrared spectrometer. The test conditions were as follows: scanning range of 4000–400 $cm^{-1}$, scanning number of 32, and resolution of 4 $cm^{-1}$.

The cross-linking density of the polymer was measured by a swelling experiment. Thermally reversible polyurethane films were cut into 7 × 7 mm thin sheets and immersed in toluene for swelling for 24 h. Before and after swelling, the composite masses were recorded as $m_0$ and $m_1$, respectively. The cross-linking density of samples was calculated according to the Flory–Rhener relation (see ESI† for details).

Tensile tests were performed on thermoreversible WPU films by a 5966 universal tensile testing machine (Instron, USA), and the healing efficiency of the polymer system was studied. The size of the samples was 20 × 4 × 0.5 ± 0.1 mm, and the speed of the tensile test head was 50 mm $min^{-1}$. At 25 °C, five parallel repeated tests were conducted for each dumbbell-shaped sample to calculate the mean values.

The WMPUS-x emulsion was diluted with water to a solid content of 1%, stirred to mix evenly and ultimately dispersed by ultrasonication. The nanoparticles were dissolved in tetrahydrofuran (THF) solution at a concentration of 10 mg/mL. The average particle size and distribution of the samples were measured at 25 °C by using dynamic light scattering (DLS, Zetasizer, Malvern Instruments).

A Phenix PH50-3A-A optical microscope was used to qualitatively observe the process of surface scratch mending and qualitatively analyze the self-healing behavior of the thermoreversible WPU films at the testing temperature of 120 °C.

Thermogravimetric analysis (TGA) of thermoreversible polyurethane films was carried out by using a TG209F1 thermal analyzer (NTEZSCH, Germany). The test conditions were as follows: 20 ml $min^{-1}$ nitrogen protection, heating rate of 10 K $min^{-1}$, and heating range of 50–800 °C. The TGA test conditions used for nanoparticles was similar to the above test conditions.

Differential scanning calorimetry (DSC) was performed on the thermoreversible WPU films by a 200 PC (NTEZSCH, Germany) differential scanning calorimeter. The curve of sample heat flow with temperature was tested and recorded. Curves were obtained by heating from −80 to 200 °C at a rate of 5 K $min^{-1}$ under a nitrogen atmosphere.

Elemental analysis (EA) was conducted by a 900 CHN (Leco, USA) elemental analyzer to test the content of S in furan@$SiO_2$.

Furan@$SiO_2$ was prepared in a 2 mg $mL^{-1}$ THF solution, and a small amount of it was dropped onto copper mesh to dry naturally. The morphology was observed by a JEM-1200EX microscope (TEM, FEI Company, USA).

Scanning electron microscopy (SEM) photos of furan@$SiO_2$ and the morphology of the fracture surface of WPU films were captured by a Quanta 250 scanning electron microscope (FEI Company, USA).

## Results and discussion

### Chemical structure of inorganic–organic hybrid nanoparticles (furan@$SiO_2$)

To date, there are many reports on the synthesis of inorganic–organic hybrid materials using TEOS and organicsiloxane substituted by functional groups as dual precursors by the sol–gel method. Many studies have confirmed the structure of the products and reaction mechanism under acid catalysis conditions [12, 13], but relatively few reports have been made under alkaline catalysis conditions. From the reaction mechanism, we hypothesized that the products after the sol–gel process under alkaline catalysis conditions were mostly dense particles. To verify the conjecture on particle structure and morphology, the final hybrid nanoparticles were further studied and characterized. SEM was used to observe the structure of hybrid particles, as shown in Fig. 1a. The organic chain segments on the surface of the particles were clean and smooth and completely covered the core. To further reveal the structure and dispersibility of furan@$SiO_2$, TEM measurements were used to observe the sample, as shown in Fig. 1b, c. It was clear that furan@$SiO_2$ was spherical in structure, with good dispersion and a certain particle size distribution. The samples all exhibited clear and transparent solutions when furan@$SiO_2$ was dispersed with solvents of different polarities with a solid content of 40% by weight (Fig. 1d). It can be speculated that the inorganic–organic hybrid nanoparticles show good dispersibility in many polar solvents due to the existence of polar chains on their shell. In addition, the DLS test [28] (Fig. S2a) yielded a more accurate particle size distribution. The FTIR spectrum showed a peak at 738 $cm^{-1}$, which was attributed to the bending vibration of the furan β-ring [29], confirming the successful synthesis of furfuryl-modified silica (Fig. S2b).

In combination with TGA and EA, the mole amount of functional groups ($c_m$) per unit gram weight of furan@$SiO_2$ could be calculated according to Eq. (1) [29].

$$c_m = \frac{100}{\Delta m_{SiO2}} \times \frac{\Delta m_S}{M_s} \times \frac{0.01}{N} \quad (1)$$

where $c_m$ is the molar concentration of functional groups per gram (mol $g^{-1}$), $\Delta m_{SiO2}$ is the residual mass of $SiO_2$ from TGA measurement (%), $\Delta m_S$ is the mass of S from EA (%), $M_S$ is the molar mass of sulfur (g $mol^{-1}$), and N is the number of sulfur atoms per functional group.

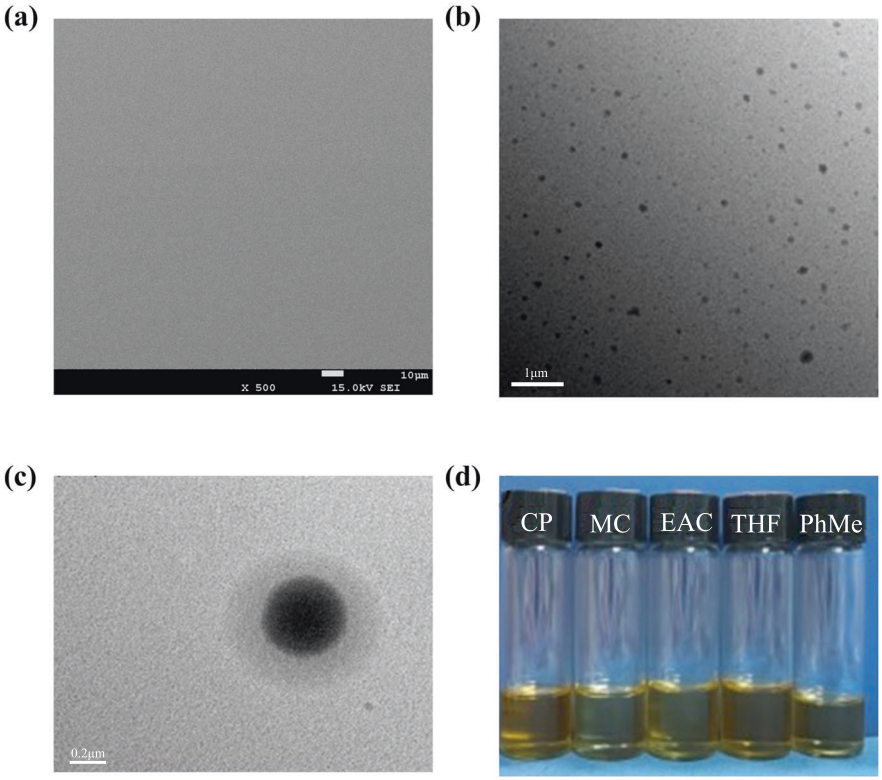


**Fig. 1** **a** SEM image of furan@$SiO_2$; **b** low-magnification and **c** high-magnification TEM images of furan@$SiO_2$; and **d** solubility of furan@$SiO_2$ in various organic solvents with a solid content of 40% by weight (CP acetone, MC dichloromethane, EAC ethyl acetate, THF tetrahydrofuran, PhMe methylbenzene)

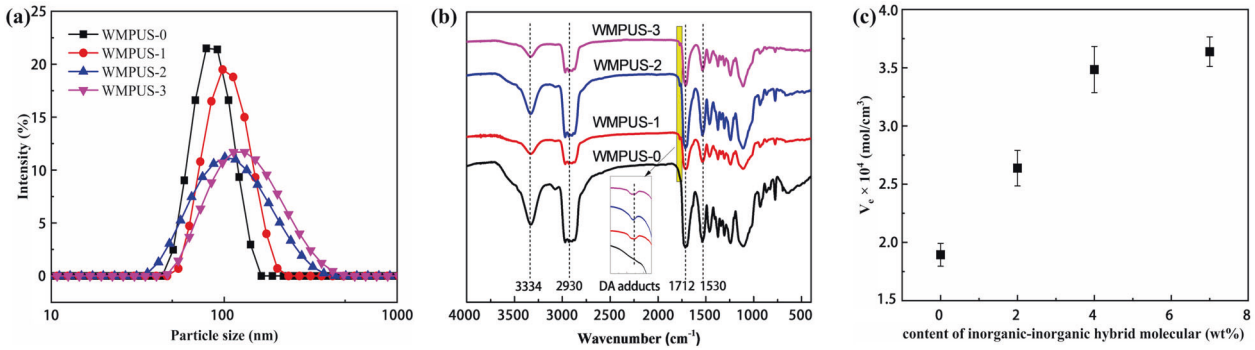


**Fig. 2** **a** Particle size and distribution of WMPUS-x emulsions; **b** FTIR transmission spectra curves of WMPUS-x films; and **c** cross-linking density of the WMPUS-x films

Detailed data are listed in Table S2. The calculated molar amount of furan groups per gram was 7.26 mmol $g^{-1}$.

Predictably, the exposure of furan groups to nanoparticles indicated that furan@$SiO_2$ can act as a reversible cross-linking agent in WPU by undergoing DA reactions with maleimides on the polymer chains and reaction with maleimide, thus improving its mechanical properties and imparting self-healing properties [30, 31]. The above results also provide ample evidence that the synthesis of furfuryl-modified silica with good dispersion can be achieved by the sol–gel method [32].

## Characterization of waterborne polyurethane (WMPUS-x)

To investigate the effect of the furan@$SiO_2$ dose on the particle size of WPU emulsions, the particle size and distribution of WMPUS-x emulsions were characterized by DLS (Fig. 2a). The particle size distribution curves of WMPUS-x emulsions revealed that there was only one peak in the particle size distributions of WMPUS-0, WMPUS-1, WMPUS-2, and WMPUS-3 emulsions, which was concentrated at 82, 98,

102, and 122 nm, respectively. The particle size of WMPUS-x emulsions increased with increasing furan@$SiO_2$ content, and the distribution progressively broadened. Possible reasons for this can be attributed to the hydrophobic behavior of furan@$SiO_2$, which causes nanoparticles to be encapsulated in the emulsified particles during the emulsification process. Meanwhile, furan@$SiO_2$ inherently exhibits a certain size distribution. Consequently, as the content of furan@$SiO_2$ in the cross-linked film increases, the extent of encapsulation in the individual emulsified particles may also increase, resulting in a larger size and wider distribution of the WMPUS-x emulsion.

The chemical structure of the WMPUS-x films was confirmed by FTIR analysis (Fig. 2b). It was not hard to observe that the WMPUS-x films had the typical polyurethane structure. The characteristic absorption peak at 1530 $cm^{-1}$ was related to the N–H bending vibration, and that at 3334 $cm^{-1}$ was attributed to the N–H stretching vibration. The absorption peak at 1712 $cm^{-1}$ corresponded to the stretching vibration of the C=O groups of urethane, and the absorption peak at 2930 $cm^{-1}$ belonged to the stretching vibration of the C–H in methyl and methylene. The above peaks indicated the successful synthesis of polyurethane [33]. As analyzed above, the main components of hybrid particles were Si–O–Si and furan rings. The characteristic antisymmetric stretching vibration peak of the Si–O–Si structure appeared at 1100 $cm^{-1}$, which was easily superimposed with the characteristic peak of ether bonds (C–O–C) on the soft segment of WPU. For the WMPUS-x film, weak characteristic peaks that corresponded to the symmetric stretching vibration of the carbonyl in DA reaction products appeared at 1772 $cm^{-1}$ [34], which further proved the successful preparation of thermo-driven self-healing WPU based on the DA reaction.

Moreover, to determine whether the addition of furan@$SiO_2$ improved the cross-linking density ($V_e$) of WPU [35], swelling experiments were carried out, and the content (x) of furan@$SiO_2$ per unit weight of WMPUS-x film was plotted against $V_e$.

According to the results shown in Fig. 2c, the following conclusions can be drawn. The $V_e$ of WMPUS-x films exhibited a positive correlation with furan@$SiO_2$ content. When the furan@$SiO_2$ content increased from 0 to 7 wt%, the cross-linking density of the WMPUS-x film increased rapidly. However, with a continuous increase in furan@$SiO_2$ content, the $V_e$ of the WMPUS-x film only increased slightly. The molar ratio of furan to maleimide reached 1:1 before the added amount of furan@$SiO_2$ reached 7%. Therefore, further increasing the furan@$SiO_2$ content had little effect on increasing the cross-linking density of WMPUS-3.

To explore the effect of furan@$SiO_2$ on the cross-sectional morphology of the polyurethane films, the WMPUS-x films were fractured by freezing in liquid nitrogen, and the morphology of the fracture surface was observed (Fig. 3). Apparently, the white circular bulges in the figure were furan@$SiO_2$. Without the addition of nanoparticles, the fracture surface of WMPUS-0 was smooth and flat, with no particle adhesion observed. However, when the furan@$SiO_2$ content increased to 2 wt%, a few white particles could be clearly observed in the cross section of the WMPUS-1 film (Fig. 3b). The interface between furan@$SiO_2$ and WPU was blurred,

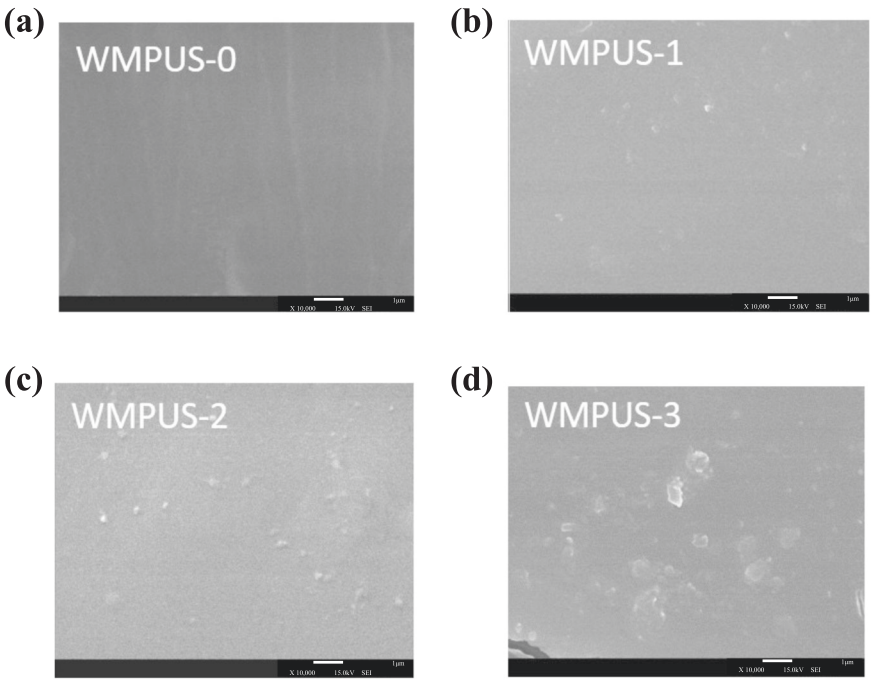


**Fig. 3** SEM images of WMPUS-x film **a** WMPUS-0; **b** WMPUS-1; **c** WMPUS-2; **d** WMPUS-3

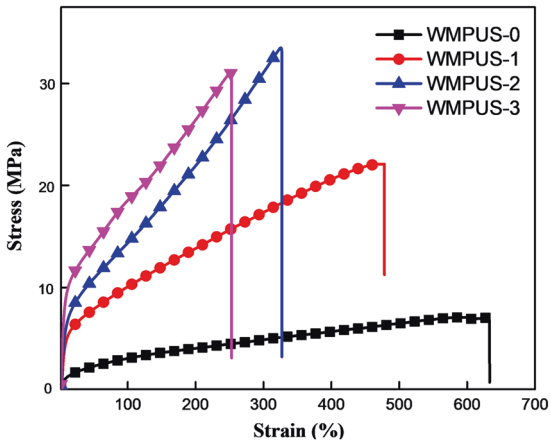


**Fig. 4** Stress-strain curves of WMPUS-x films

and a significant quantity of furan@$SiO_2$ was buried deep in the substrate layer. These phenomena indicate that the DA reaction between furan@$SiO_2$ and WPU enhances the mutual interfacial interaction. As the furan@$SiO_2$ content increased to 7 wt%, the particles in the cross section of the WMPUS-3 film increased, and obvious agglomeration occurred (Fig. 3d). When the molar ratio of furan and maleimide groups was large, some furan@$SiO_2$ could not participate in the reaction, the interfacial interaction between furan@$SiO_2$ and the polymer matrix was weakened, and local agglomeration occurred. During the emulsification process, furan@$SiO_2$ was encapsulated in polyurethane emulsion particles. As the water evaporated, capillary action forced the emulsion particles to deform until the interface between emulsion particles disappeared, eventually forming a film. In this process, the maleimide-furan reaction could effectively abate the agglomeration phenomenon. When the amount of furan@$SiO_2$ was large, owing to the aggregation tendency of nanoparticles, aggregation occurred before the maleimide-furan reaction, which led to the unsmooth surface of the WMPUS-x films [36, 37]. The above evidence indicates that the compatibility of furan@$SiO_2$ and WPU is excellent. Combined with the characterization of hybrid particles above, we can reasonably infer that this is due to the high grafting rate of organic groups in furan@$SiO_2$. However, furan@$SiO_2$ can agglomerate in WPU at a high content, which might eventually affect the comprehensive properties of the composite.

The mechanical properties of the WMPUS-x films were characterized, as shown in Fig. 4 and detailed in Table 1. As shown in Fig. 4, the tensile strength of the WMPUS-x films trended upwards and then downwards with increasing furan@$SiO_2$ content, while the elongation at break decreased and the Young's modulus continuously increased. The rigid cores of furan@$SiO_2$ in the WMPUS-x film improved the tensile strength and Young's modulus, while the DA reaction reinforced the interfacial interaction between

**Table 1** Details from the stress-strain curves of WMPUS-x films

| Sample | Stress/MPa | Strain/% | Modulus/MPa |
|---|---|---|---|
| WMPUS-0 | 6.5 ± 1.2 | 635.7 ± 30.6 | 6.2 ± 1.3 |
| WMPUS-1 | 20.2 ± 3.1 | 480.4 ± 29.5 | 30.9 ± 2.2 |
| WMPUS-2 | 30.9 ± 3.9 | 326.7 ± 18.3 | 58.7 ± 6.0 |
| WMPUS-3 | 28.7 ± 3.9 | 249.9 ± 19.6 | 76.5 ± 6.5 |

furan@$SiO_2$ and polyurethane. The load energy could be transferred effectively during the tensile process, which further improved the tensile strength of the WMPUS-x films. However, when the furan@$SiO_2$ content increased to 7 wt%, agglomeration of furan@$SiO_2$ in the WMPUS-3 film occurred and was accompanied by a slight decrease in tensile strength due to stress concentration [38, 39]. Furthermore, the cross-linking density of WMPUS-x films improved as the furan@$SiO_2$ content increased. For the elongation at break, the more chemical cross-linking points there are, the greater the movement ability of the polymer chain is hindered. Additionally, furan@$SiO_2$ had a certain physical entanglement effect on the polymer chain, so the cross-linking density of the WMPUS-x films increased with increasing furan@$SiO_2$ content. As a result, the elongation at break of the WMPUS-3 film gradually decreased as the furan@$SiO_2$ content increased.

Thermal stability is an important part of WPU research. Figure 5 shows the TGA and DTG curves of WMPUS-x films. As seen in Fig. 5a, the temperature $T_{5\%}$ (5% mass loss temperature) of the WMPUS-x films gradually increased with increasing furan@$SiO_2$ content. The thermal decomposition of WMPUS-x films could be divided into two stages (Fig. 5b): the first stage was the thermal degradation of hard-segment carbamate groups in the range of 280–340 °C, and the second stage was the thermal degradation of soft-segment ether bonds at ~340–420 °C [40, 41]. Notably, the thermal degradation temperatures of the hard and soft segments shifted toward higher temperatures due to the incorporation of furan@$SiO_2$. When the content of furan@$SiO_2$ increased from 2 to 7 wt%, the maximum decomposition rates of the hard and soft segments increased from 302 °C and 311 °C to 377 °C and 388 °C, respectively. Based on the above analysis, it is evident that the addition of furan@$SiO_2$ can effectively improve the thermal stability of WMPUS-0.

## Thermal reversibility and self-healing behavior of WMPUS-x films

DSC was used to analyze the thermally reversible temperature of the WMPUS-x films. Figure 6a shows the DSC curve of WMPUS-x films. A broad endothermic peak belonging to the retro-DA reaction could be observed in the DSC heating curves of WMPUS-x films in the range of

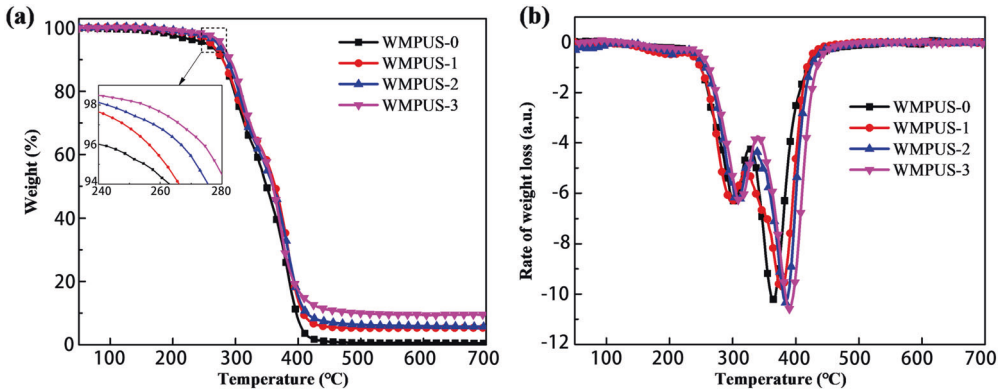


**Fig. 5** **a** TGA curves and **b** DTG thermograms of WMPUS-x films

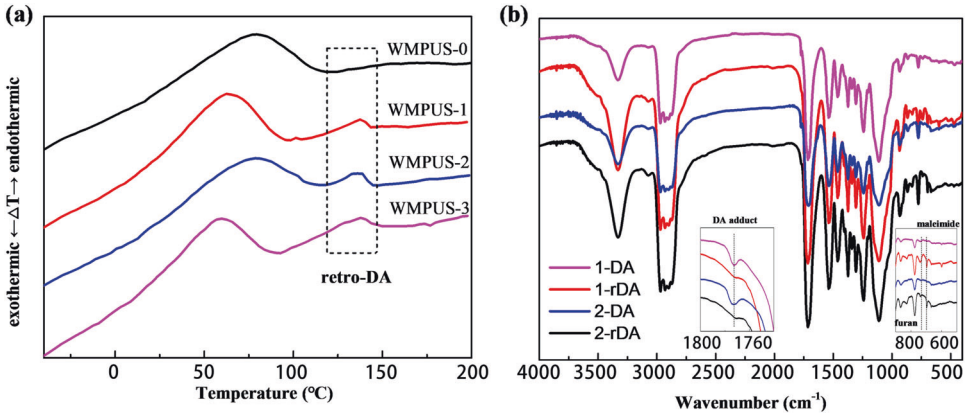


**Fig. 6** Thermal-induced reversible behavior of WMPUS-x films. **a** DSC curves of WMPUS-x films. **b** FTIR transmission spectra of the WMPUS-2 film before and after multiple DA and retro-DA reactions

120–150 °C. This peak did not appear in the DSC curve of WMPUS-0 since there was no cross-linking point of the DA reaction. These phenomena indicate the thermally reversible behavior of WMPUS-x films corresponding to temperatures of 120–150 °C. The peaks between 40 and 100 °C were related to the melting process of the hard segment.

The structural changes of the WMPUS-2 film before and after the thermal reversible reaction were compared by FTIR to analyze the thermally reversible behavior mechanism, and the relevant curves are shown in Fig. 6b. First, the WMPUS-2 film with a thickness of 0.1 ± 0.05 mm was examined by FTIR, and the correlation curve (1-DA) was recorded. Then, the WMPUS-2 film was heated at 130 °C for 10 min for retro-DA reaction, and the FTIR spectrum curve (1-rDA) was recorded at room temperature. Subsequently, the WMPUS-2 film was subjected to a DA reaction by heating at 65 °C for 20 min, and the FTIR spectrum curve (2-DA) was measured. Eventually, the FTIR spectrum curve (2-rDA) of the WMPUS-2 film was measured under the same reaction conditions as the first retro-DA reaction. As seen from the figure, the symmetric stretching vibration peak of the carbonyl group belonging to the DA adduct at 1772 $cm^{-1}$ could be clearly observed on the 1-DA curve, without the characteristic peaks of furan and maleimide appearing. However, after the first retro-DA reaction, new characteristic peaks appeared at 738 and 696 $cm^{-1}$, corresponding to the bending vibration of the furan β-ring and the stretching vibration of the maleimide cis dihydrogen in the double bond, respectively [42]. Moreover, faint characteristic peaks attributed to the DA adduct could still be observed, indicating that the DA cross-linking points had not been completely cleaved at this stage. Following recrosslinking of the film, the 2-DA curve of the WMPUS-2 film revealed a distinct DA adduct structure again, accompanied by a reduction in or even disappearance of the intensity of the characteristic peaks of furan and maleimide. Particularly, after a second retro-DA reaction, the intensity of the DA adduct decreased significantly, and the characteristic peaks of the furan ring and maleimide reappeared, indicating that the cross-linking points of the DA reaction were broken into a mixture of nanoparticles with furan and maleimide-terminated polyurethane chains. In addition, the structure of polyurethane and hybrid nanoparticles did not change, even after the WMPUS-2 film experienced several thermally reversible reactions. The above result demonstrates that the thermal reversible behavior of the WMPUS-x cross-linked film is attributed to the presence of reversible cross-linking sites with the DA reaction. Therefore, the film is able to return to its original structure after multiple reversible cross-linking reactions [43, 44].

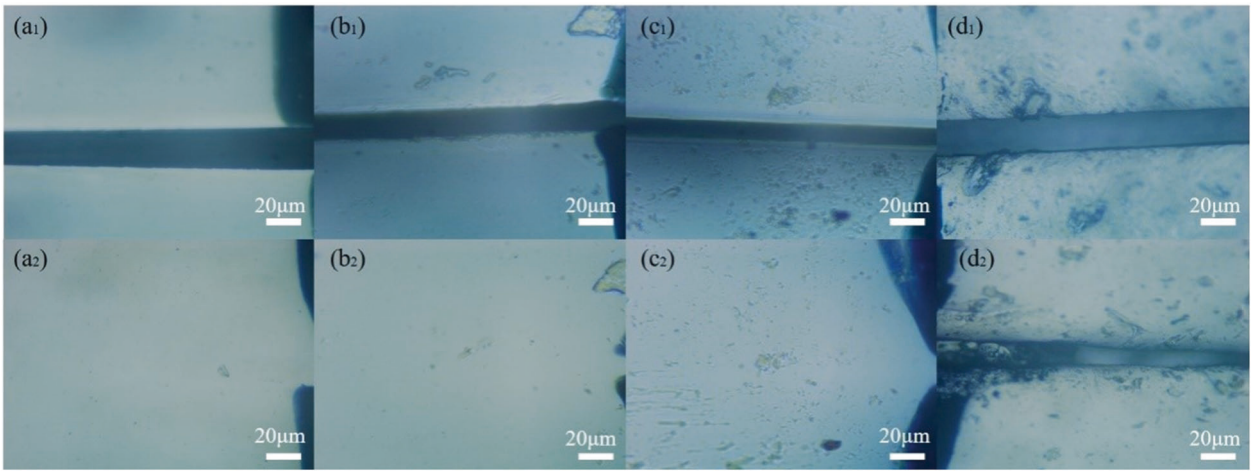


**Fig. 7** Optical microscope images of the incisions on the surfaces of cross-linked **a** WMPUS-1, **b** WMPUS-2, **c** WMPUS-3 and **d** WMPUS-0 films before ($a_1$, $b_1$, $c_1$, $d_1$) and after thermotriggered self-healing at 130 °C for 5 min ($a_2$, $b_2$, $c_2$, $d_2$)

The self-healing properties of WMPUS-x films were qualitatively evaluated by an optical microscope. A 20 μm incision was made in the WMPUS-x films with a blade, and then, the films were placed under an optical microscope with a hot stage at 130 °C. The self-healing process lasted 5 min, and images of the incision before ($a_1$, $b_1$, $c_1$, $d_1$) and after self-healing ($a_2$, $b_2$, $c_2$, $d_2$) were captured (Fig. 7). The crack of WMPUS-0 narrowed under this condition without complete healing ($d_1$ and $d_2$), while the cracks of WMPUS-1, WMPUS-2, and WMPUS-3 (shown in Fig. 7($a_1$, $b_1$, and $c_1$), respectively) were completely filled to form a complete whole with the surroundings (shown in Fig. 7($a_2$, $b_2$, and $c_2$), respectively). WMPUS-0 has a straight chain polyurethane structure, and high temperature can promote the movement of long polyurethane chains. However, due to the lack of DA reversible cross-linking points, the crack width was relatively reduced, but the crack could not completely disappear during short-term heating for only 5 min. At this time, the DA cross-linking points in WMPUS-1, WMPUS-2 and WMPUS-3 were subjected to retro-DA reaction, and the cross-linked films were degraded into maleimide-terminated polyurethane chains and hybrid nanoparticles. The enhanced mobility of the molecules, which can move freely at high temperature, enabled rapid filling of cracks and macroscopic healing. These results verify that the existence of DA reversible cross-linking points is the key factor for the WMPUS-x film to self-heal.

### Healing behavior of the mechanical properties of WMPUS-x films

Since the cross-linking points can repeatedly undergo DA/retro-DA reactions, WMPUS-x films can undergo self-healing several times. To investigate whether the mechanical properties of WMPUS-x films can be recovered after repeated healing, the following treatment was carried out: The samples were cut into dumbbell-shaped standard strips, cut down the middle, macrobonded and placed in an oven at 130 °C for 10 min and then at 65 °C for 8 h. To assess the tensile strength of WMPUS-x after the healing process, the first self-healing tensile test was performed followed by a second self-healing tensile test in which the above procedure was repeated twice on the specimen. The stress-strain curves of WMPUS-x films after multiple healing processes are shown in Fig. 8. The first self-healing efficiencies (Fig. 8a) of the WMPUS-1, WMPUS-2, and WMPUS-3 films were 88.4%, 89.3 and 88.1%, respectively, while the second healing efficiencies were 80.9%, 81.9 and 78.6%, respectively (the error bars were calculated from the sample variance). Because the reversible cross-linking points of DA are not fully recovered under these conditions and agglomeration of furan@$SiO_2$ might be caused at high temperature, the second healing efficiency is reduced compared to the first.

## Conclusions

In summary, homogeneously dispersed furfuryl-modified silica nanoparticles were successfully synthesized and introduced into emulsions of maleimide-terminated WPU. By DA/retro-DA reaction, a thermoreversible dynamic cross-linking network was constructed between the inorganic phase and organic phase by using furan@$SiO_2$ as dynamic cross-linking points, and WMPUS-x films with thermoreversible dynamic cross-linking structures were prepared. It has been corroborated that the structure can significantly enhance the interfacial

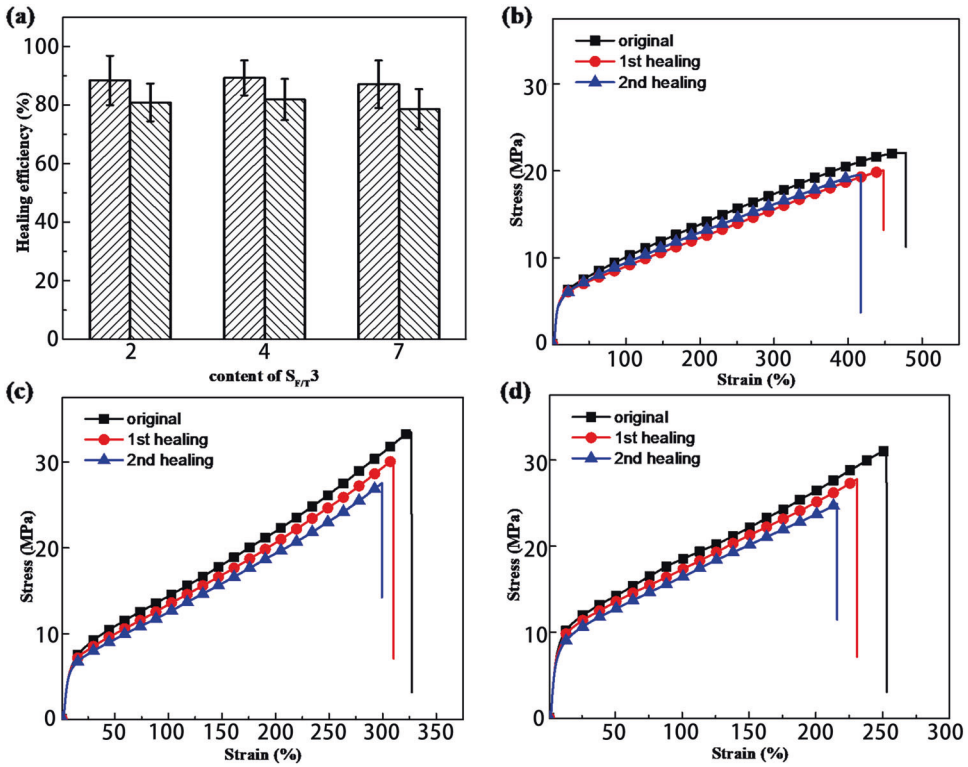


**Fig. 8** Self-healing properties of WMPUS-x films. **a** Healing efficiency of WMPUS-x films. Stress-strain curves before and after the healing of **b** WMPUS-1, **c** WMPUS-2 and **d** WMPUS-3 films

force among furan@$SiO_2$ and WPU, and finally, reinforced composites with comprehensive performance were obtained. Moreover, the mechanical properties of WMPUS-1, WMPUS-2 and WMPUS-3 were significantly enhanced compared with those of WMPUS-0, despite the local aggregation phenomenon of hybrid nanoparticles in WMPUS-3. Furthermore, from the tensile tests, WMPUS-x showed efficient self-healing performance, even after being physically damaged multiple times. The above conclusion confirms that the combination of an organic phase and an inorganic phase by chemical cross-linking is a considerable way to reinforce mechanical properties and endow polymers with self-healing ability, which will play an important role in future research.

**Acknowledgements** This work was funded by the National Natural Science Foundation of China (No. 51773129 and 51903167), the Support Plan of the Science and Technology Department of Sichuan Province, China (2020YFG0071, 22ZDYF3307), the Opening Project of the Key Laboratory of Leather Chemistry and Engineering, (Sichuan University), and the Ministry of Education (SCU2021D005). The authors thank Zhonghui Wang for her great help in FT-IR/TEM analyzer observation.

## Compliance with ethical standard

**Conflict of interest** The authors declare no competing interests.

**Publisher's note** Springer Nature remains neutral with regard to jurisdictional claims in published maps and institutional affiliations.

## References

1. Shin M, Lee Y, Rahman M, Kim H. Synthesis and properties of waterborne fluorinated polyurethane-acrylate using a solvent-/emulsifier-free method. Polymer. 2013;54:4873–82.
2. Ji X, Wang H, Ma X, Hou C, Ma G. Progress in polydimethylsiloxane-modified waterborne polyurethanes. Rsc Adv. 2017;7:34086–95.
3. Yang W, Cheng X, Wang HB, Liu YS, Du ZL. Surface and mechanical properties of waterborne polyurethane films reinforced by hydroxyl-terminated poly(fluoroalkyl methacrylates). Polym. 2017;133:68–77.
4. Zhang SW, Ren LIU, Jiang JQ, Yang C, Chen MQ, Liu XY. Facile synthesis of waterborne UV-curable polyurethane/silica nanocomposites and morphology, physical properties of its nanostructured films. Prog Org Coat. 2011;70:1–8.
5. Abdollahi A, Roghani-Mamagani H, Salami-Kalajahi M, Mousavi A, Razavi B, Shahi S. Preparation of organic-inorganic hybrid nanocomposites from chemically modified epoxy and novolac resins and silica-attached carbon nanotubes by sol-gel process: Investigation of thermal degradation and stability. Prog Org Coat. 2018;117:154–65.
6. Akram D, Hakami O, Sharmin E. Ahmad S. Castor and Linseed oil polyurethane/TEOS hybrids as protective coatings: A synergistic approach utilising plant oil polyols, a sustainable resource. Prog Org Coat. 2017;108:1–14.
7. Liu YL, Hsu CY, Wang ML, Chen HS. A novel approach of chemical functionalization on nano-scaled silica particles. Nanotech. 2003;14:813–9.
8. Xie LH, Yin CR, Lai WY, Fan QL, Huang W. Polyfluorene-based semiconductors combined with various periodic table elements for organic electronics. Prog Polym Sci. 2012;37:1192–264.
9. Lee M, Kim JU, Lee JS, Lee BI, Shin J, Park CB. Mussel-inspired plasmonic nanohybrids for light harvesting. Adv Mater. 2014;26:4463–8.

10. Engel T, Kickelbick G. Self-healing nanocomposites from silica – polymer core – shell nanoparticles. Polym Int. 2014;63:915–23.
11. Huang ZW, Wang Y, Zhu J, Yu JR, Hu ZM. Surface engineering of nanosilica for vitrimer composites. Compos Sci Technol. 2018;154:18–27.
12. Zhou H, Xue W, Li F, Qin Y. Study on the Sol-gel Process of TEOS by React-IR. Appl Mech Mater. 2012;110:1401–5.
13. Ciriminna R, Fidalgo A, Pandarus V, Beland F, Ilharco LM, Pagliaro M. The Sol-Gel Route to Advanced Silica-Based Materials and Recent Applications. Chem Rev. 2013;113:6592–620.
14. Prabakar S, Assink RA. Hydrolysis and condensation kinetics of two component organically modified silica sols. J Non-Crys Solids. 1997;211:39–48.
15. Brus J, Dybal J. Copolymerization of tetraethoxysilane and dimethyl(diethoxy)silane studied by Si-29 NMR and ab initio calculations of Si-29 NMR chemical shifts. Polymer. 1999;40:6933–45.
16. Zhang Y, Ying H, Hart KR, Wu Y, Hsu AJ, Coppola AM, et al. Malleable and recyclable poly(urea-urethane) thermosets bearing hindered urea bonds. Adv Mater. 2016;28:7646–51.
17. Cuevas JM, Seoane-Rivero R, Navarro R, Marcos-Fernández Á. Coumarins into polyurethanes for smart and functional materials. Polymers. 2020;12:630.
18. Xu WM, Rong MZ, Zhang MQ. Sunlight driven self-healing, reshaping and recycling of a robust, transparent and yellowing-resistant polymer. J Mater Chem A. 2016;4:10683–90.
19. Li CH, Wang C, Keplinger C, Zuo JL, Jin L, Sun Y, et al. A highly stretchable autonomous self-healing elastomer. Nat Chem. 2016;8:618–24.
20. Chen X, Dam MA, Ono K, Mal A, Shen H, Nutt SR, et al. A thermally re-mendable cross-linked polymeric material. Science 2002;295:1698–702.
21. Huang N, Ding X, Kim J, Ihee H, Jiang D. A photoresponsive smart covalent organic framework. Angew Chem Int Ed 2015;54:8704–7.
22. Aguirresarobe RH, Irusta L, Fernández-Berridi MJ. UV-light responsive waterborne polyurethane based on coumarin: synthesis and kinetics of reversible chain extension. J Polym Res. 2014;21:505.
23. Xu Y, Chen D. A novel self-healing polyurethane based on disulfide bonds. Macromol Chem Phys. 2016;217:1191–6.
24. Adzima BJ, Aguirre HA, Kloxin CJ, Scott TF, Bowman CN. Rheological and chemical analysis of reverse gelation in a covalently cross-linked Diels−Alder polymer network. Macromolecule 2008;41:9112–7.
25. Li J, Zhang G, Deng L, Zhao S, Gao Y, Jiang K, et al. In situ polymerization of mechanically reinforced, thermally healable graphene oxide/polyurethane composites based on Diels–Alder chemistry. J Mater Chem A. 2014;2:20642–9.
26. Bai N, Saito K, Simon GP. Synthesis of a diamine cross-linker containing Diels–Alder adducts to produce self-healing thermosetting epoxy polymer from a widely used epoxy monomer. Polym Chem. 2013;4:724–30.
27. Pu W, Fu D, Wang Z, Gan X, Lu X, Yang L, et al. Realizing crack diagnosing and self-healing by electricity with a dynamic cross-linked flexible polyurethane composite. Adv Sci. 2018;5:1800101.
28. Xu Y, Wu D, Sun Y, Chen W, Yuan H, Deng F, et al. Effect of polyvinylpyrrolidone on the ammonia-catalyzed sol-gel process of TEOS: Study by in situ Si-29 NMR, scattering, and rheology. Colloid Surf A. 2007;305:97–104.
29. Engel T, Kickelbick G. Thermoreversible reactions on inorganic nanoparticle surfaces: diels-alder reactions on sterically crowded surfaces. Chem Mater. 2013;25:149–57.
30. Wu J, Cai LH, Weitz DA. Tough self-healing elastomers by molecular enforced integration of covalent and reversible networks. Adv Mater. 2017;29:1702616.
31. Ruckenstein E, Chen XN. Covalent cross-linking of polymers through ionene formation and their thermal de-cross-linking. Macromolecule. 2000;33:8992–9001.
32. Young SK, Jarrett WL, Mauritz KA. Nafion (R)/ORMOSIL nanocomposites via polymer-in situ sol-gel reactions. 1. Probe of ORMOSIL phase nanostructures by Si-29 solid-state NMR spectroscopy. Polymer 2002;43:2311–20.
33. Fang Y, Du X, Jiang Y, Du Z, Pan P, Cheng X, et al. Thermal-driven self-healing and recyclable waterborne polyurethane films based on reversible covalent interaction. ACS Sustain Chem Eng. 2018;6:14490–500.
34. Khan NI, Halder S, Wang J. Diels-Alder based epoxy matrix and interfacial healing of bismaleimide grafted GNP infused hybrid nanocomposites. Polym Test. 2019;74:138–51.
35. Mahdi EM, Tan JC. Dynamic molecular interactions between polyurethane and ZIF-8 in a polymer-MOF nanocomposite: Microstructural, thermo-mechanical and viscoelastic effects. Polymer. 2016;97:31–43.
36. Yang S, Liu J, Pan F, Yin X, Wang L, Chen D, et al. Fabrication of self-healing and hydrophilic coatings from liquid-like graphene@SiO2 hybrids. Compos Sci Technol. 2016;136:133–44.
37. Yang S, Li S, Yin X, Wang L, Chen D, Zhou Y, et al. Preparation and characterization of non-solvent halloysite nanotubes nanofluids. Appl Clay Sci. 2016;126:215–22.
38. Zhang Y, Wang Q, Wang C, Wang T. High-strain shape memory polymer networks crosslinked by SiO2. J Mater Chem. 2011;21:9073–8.
39. Chen TK, Tien YI, Wei KH. Synthesis and characterization of novel segmented polyurethane/clay nanocomposites. Polymer. 2000;41:1345–53.
40. Hui B, Ye L. Highly heat-resistant silicon-containing polyurethane-imide copolymers: Synthesis and thermal mechanical stability. Eur Polym J. 2017;91:337–53.
41. Zhang P, Fan H, Hu K, Gu Y, Chen Y, Yan J, et al. Solvent-free two-component polyurethane conjugated with crosslinkable hydroxyl-functionalized ammonium polyphosphate: Curing behaviors, flammability and mechanical properties. Prog Org Coat. 2018;120:88–99.
42. Thuy TT, Son HT, Ha TN, Dung TTP, Loc TN, Hung QP, et al. Tailoring the Hard-Soft Interface with Dynamic Diels-Alder Linkages in Polyurethanes: Toward Superior Mechanical Properties and Healability at Mild Temperature. Chem Mater. 2019;31:2347–57.
43. Zhao J, Xu R, Luo G, Wu J, Xia H. A self-healing, re-moldable and biocompatible crosslinked polysiloxane elastomer. J Mater Chem B. 2016;4:982–9.
44. Feng L, Yu Z, Bian Y, Lu J, Shi X, Chai C. Self-healing behavior of polyurethanes based on dual actions of thermo-reversible Diels-Alder reaction and thermal movement of molecular chains. Polymer. 2017;124:48–59.